

Geometrical resonances in a high-injection-current nonequilibrium state of superconductor—normal-metal contacts

Artur Hahn

Institut für Werkstoffe der Elektrotechnik, Ruhr-Universität Bochum, D-4630 Bochum-Querenburg, Federal Republic of Germany

(Received 16 August 1984)

A hysteretic transition to a high-injection-current nonequilibrium state in metallic contacts between silver and high-purity single-crystal tantalum was recently observed by the author and H. Lerchner. Oscillations of conductance with bias in this state are interpreted as geometrical resonances of the excess current caused by a bias-driven variation of the superconductor—normal-metal phase-boundary position. Quantitative numerical results are obtained from an extension of the one-dimensional Blonder-Tinkham-Klapwijk microconstriction model and are successfully compared with part of the experimental results. Lacking any self-consistency features, the model is unable to describe nonlinearities and feedback effects which apparently dominate much of the experimental behavior, but supplies some indication that Andreev reflection might also play an essential role in these effects.

I. INTRODUCTION

In a previous paper,¹ referred to as HL in the following, the author and H. Lerchner reported observations of a high-injection-current state in superconductor—normal-metal metallic contacts. This state was characterized by a conductance oscillating with applied bias, and it was separated from a smooth low-injection-current behavior by a hysteretic transition. The low-injection-current behavior, on the other hand, roughly followed the expectation from the superconductor—normal-metal microconstriction model given by Blonder *et al.*,² referred to as BTK in HL and in this paper.

In HL some formulas were given, derivable from a simple extension of the BTK model leading to an oscillatory dependence of the excess current at high voltage U ,

$$I_{\text{exc}}(U) = I_S(U) - R_N^{-1}U, \quad (1)$$

on what was called the “melting depth” l of the superconductor. Here, $I_S(U)$ is the current with superconductivity established in the superconducting bank, and $R_N^{-1}U$ is the current with superconductivity suppressed by a magnetic field or by a temperature above T_c i.e., R_N is the resistance of the junction in the normal state. The idea in HL was that heating effects in our low-resistance ($R_N < 1 \Omega$) contacts give rise to suppression of the pair potential within a finite depth l below the surface of the superconducting bank, with l increasing with bias. Attempting to retain the simplicity of the one-dimensional BTK model and approximating the normal and pair potentials by Θ functions, one arrives at a model within which the discontinuities of the normal and of the pair potentials are separated by the finite length l . Clearly, interference effects for the transmission and reflection coefficients must be expected in this situation on account of the well-known mechanism of combined normal and Andreev³ reflection.

In Sec. II the theoretical result is derived, which was

only stated by HL without derivation.⁴ The result is valid under somewhat more general conditions and can be expressed in a more concise form [Eqs. (18)–(20) below] than given previously. Section III contains a report on sample preparation and experimental results beyond that given in HL. HL presented an example of high-injection-current characteristics with oscillating behavior of differential conductance in the high-injection-current regime. Meanwhile, a detailed numerical analysis of this example was performed on the basis of the proposed theory. Section IV contains this analysis, together with more information on numerical consequences of the model. A final discussion of physical parameters resulting from the analysis is given in Sec. V.

II. CURRENT-TRANSMISSION COEFFICIENT FOR A ONE-DIMENSIONAL NORMAL-NORMAL-SUPERCONDUCTING GEOMETRY

The techniques given by BTK are simply adopted to calculate the energy-dependent quasiparticle current-transmission coefficient $T(E)$ on the basis of the Bogoliubov equations^{5,6} for the wave function

$$\psi(x) = \begin{bmatrix} u(x) \\ v(x) \end{bmatrix},$$

namely

$$\left[-\frac{\hbar^2}{2m} \frac{d^2}{dx^2} + V(x) - \epsilon_F \right] u(x) + \Delta(x)v(x) = Eu(x), \quad (2)$$

$$-\left[-\frac{\hbar^2}{2m} \frac{d^2}{dx^2} + V(x) - \epsilon_F \right] v(x) + \Delta(x)u(x) = Ev(x).$$

The normal and pair potentials $V(x)$ and $\Delta(x)$, respectively, are assumed as given in Fig. 1, the singularities of $V(x)$ at $x=0$ being given by a δ function of strength H and a step which we describe by different values of Fermi wave numbers and Fermi velocities, $k_F^<$, $k_F^>$, $v_F^<$, and $v_F^>$ for $x \leq 0$, respectively. Physically, $x=0$ corresponds to the contact between the two metals, the normal metal filling the half-space $x < 0$. In the second metal, the pair potential is destroyed by current injection down to the depth l . The case $l=0$ corresponds to BTK, from which much of the treatment is directly adopted, including details of notation. Instead of mentioning this at every instance, we emphasize here that nothing else is new in this section, but introduce the finite "melting depth" l which separates the normal and pair potential discontinuities, and solve an 8×8 linear-equation system for the scattered-wave amplitudes instead of a 4×4 system.

Normalizing the amplitude of an electronlike excitation reaching the contact from the left to 1, the ansatz to solve Eqs. (2) is

$$\psi(x) = \begin{cases} \begin{pmatrix} 1 \\ 0 \end{pmatrix} e^{iq^+x} + b \begin{pmatrix} 1 \\ 0 \end{pmatrix} e^{-iq^+x} + a \begin{pmatrix} 0 \\ 1 \end{pmatrix} e^{iq^-x} & \text{for } x < 0, \\ e \begin{pmatrix} 1 \\ 0 \end{pmatrix} e^{ik^+x} + f \begin{pmatrix} 1 \\ 0 \end{pmatrix} e^{-ik^+x} + h \begin{pmatrix} 0 \\ 1 \end{pmatrix} e^{ik^-x} + g \begin{pmatrix} 0 \\ 1 \end{pmatrix} e^{-ik^-x} & \text{for } 0 < x < l, \\ c \begin{pmatrix} u_0 \\ v_0 \end{pmatrix} e^{i\kappa^+x} + d \begin{pmatrix} v_0 \\ u_0 \end{pmatrix} e^{-i\kappa^-x} & \text{for } x > l, \end{cases} \quad (3)$$

with

$$\begin{aligned} q^\pm &= k_F^\pm \pm E/\hbar v_F^\pm, \\ k^\pm &= k_F^\pm \pm \frac{1}{2} \delta k(E), \quad \frac{1}{2} \delta k(E) = E/\hbar v_F^\pm, \\ \kappa^\pm &= +(2m)^{1/2} \hbar^{-1} [\epsilon_F \pm (E^2 - \Delta^2)^{1/2}]^{1/2}. \end{aligned} \quad (4)$$

To guarantee outgoing or damped quasiparticles for $x > l$, the κ^\pm must be taken with positive real parts in any case, and, for $E < \Delta$, with positive or negative imaginary parts for the upper and lower sign, respectively. The coherence factors have the usual form,

$$\begin{pmatrix} -1 & 0 & 1 & 0 & 1 & 0 & 0 & 0 \\ r+2iZ^0 & 0 & 1 & 0 & -1 & 0 & 0 & 0 \\ 0 & -1 & 0 & 1 & 0 & 1 & 0 & 0 \\ 0 & -r+2iZ^0 & 0 & 1 & 0 & -1 & 0 & 0 \\ 0 & 0 & e^{ik^+l} & 0 & e^{-ik^+l} & 0 & -u_0 & -v_0 \\ 0 & 0 & e^{i\kappa^+l} & 0 & -e^{-i\kappa^+l} & 0 & -u_0 & v_0 \\ 0 & 0 & 0 & e^{ik^-l} & 0 & e^{-ik^-l} & -v_0 & -u_0 \\ 0 & 0 & 0 & e^{i\kappa^-l} & 0 & -e^{-i\kappa^-l} & -v_0 & u_0 \end{pmatrix} \begin{pmatrix} b \\ a \\ e \\ h \\ f \\ g \\ c e^{i\kappa^+l} \\ d e^{-i\kappa^-l} \end{pmatrix} = \begin{pmatrix} 1 \\ r-2iZ^0 \\ 0 \\ 0 \\ 0 \\ 0 \\ 0 \\ 0 \end{pmatrix}. \quad (7)$$

Here, r and Z^0 are given by

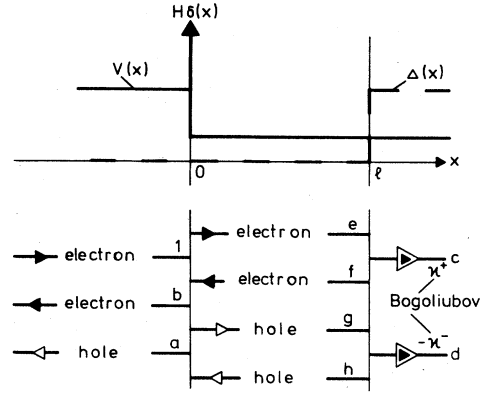


FIG. 1. Upper part: Normal and pair potentials defining the model for calculation of the energy-dependent current-transmission coefficient. Lower part: Amplitudes a, \dots, h and group-velocity directions of the outgoing quasiparticle waves produced by an incoming electronlike quasiparticle excitation within the BTK scheme.

$$u_0^2 = 1 - v_0^2 = \frac{1}{2} [1 + E^{-1} (E^2 - \Delta^2)^{1/2}], \quad (5)$$

their definition being extended by BTK to $E < \Delta$, for which case u_0^2 and v_0^2 are thus complex conjugates.

While the ansatz guarantees solution of the Bogoliubov equations within the three regions, the boundary conditions,

$$\psi(0^+) - \psi(0^-) = 0, \quad \psi(l^+) - \psi(l^-) = 0, \quad (6)$$

$$\psi'(0^+) - \psi'(0^-) = (2m/\hbar^2) H \psi(0), \quad \psi'(l^+) - \psi'(l^-) = 0,$$

determine the eight coefficients a, \dots, h . We obtain

$$r = \frac{k_F^<}{k_F^>} = \frac{v_F^<}{v_F^>} \quad \text{and} \quad Z^0 = mH/\hbar^2 k_F^>. \quad (8)$$

The quantities q^\pm , k^\pm , and κ^\pm were replaced by $k_F^<$, $k_F^>$, and $k_F^>$, respectively, at the places where they appeared as factors from taking the derivative, but k^+ and k^- must be retained in the phases where their difference leads to the interference effects we are interested in.

On account of current continuity, the amplitudes at any fixed x are sufficient to determine the current-transmission coefficient. Again following BTK, we determine the coefficients in the $x < 0$ bank, i.e., we eliminate from (7) all coefficients except a and b . The algebra is straightforward and need not be given here. The result is

$$\begin{aligned} b &= (4rD)^{-1}(r+1-2iZ^0)(r-1-2iZ^0)(v_0^2 e^{i\alpha} - u_0^2 e^{-i\alpha}), \\ a &= (4rD)^{-1}(-4ru_0 v_0), \\ 4rD &= (r-1+2iZ^0)(r-1-2iZ^0)v_0^2 e^{i\alpha} - (r+1+2iZ^0)(r+1-2iZ^0)u_0^2 e^{-i\alpha}, \end{aligned} \quad (9)$$

with

$$\alpha = l \delta k(E). \quad (10)$$

To square the amplitudes, it is convenient to introduce a phase $\phi = \phi(E)$ by

$$u_0^2 = |u_0|^2 e^{i\phi}, \quad v_0^2 = |v_0|^2 e^{-i\phi}, \quad (11)$$

where, from (5),

$$\phi = \begin{cases} 0 & \text{for } E > \Delta, \\ \arccos(E/\Delta) & \text{for } E < \Delta. \end{cases} \quad (12)$$

After some algebra, we obtain

$$\begin{aligned} |b|^2 &= |D|^{-2} \left[\frac{(r-1)^2}{4r} + Z^2 \right] \left[\frac{(r+1)^2}{4r} + Z^2 \right] \{ |u_0|^4 + |v_0|^4 - 2|u_0|^2 |v_0|^2 \cos[2(\alpha - \phi)] \}, \\ |a|^2 &= |D|^{-2} |u_0|^2 |v_0|^2, \\ |D|^2 &= \left[\frac{(r-1)^2}{4r} + Z^2 \right]^2 |v_0|^4 + \left[\frac{(r+1)^2}{4r} + Z^2 \right]^2 |u_0|^4 \\ &\quad - 2 \left[\frac{(r-1)^2}{4r} + Z^2 \right] \left[\frac{(r+1)^2}{4r} + Z^2 \right] |u_0|^2 |v_0|^2 \cos[2(\alpha - \phi)], \end{aligned} \quad (13)$$

with

$$Z = r^{-1/2} Z^0 = \frac{mH}{\hbar^2 (k_F^> k_F^<)^{1/2}} = \frac{H}{\hbar (v_F^> v_F^<)^{1/2}}. \quad (14)$$

Since

$$\frac{(r+1)^2}{4r} = \frac{(r-1)^2}{4r} + 1,$$

Eq. (13) is suited to demonstrate that $|a|^2$ and $|b|^2$, and hence the current-transmission coefficient, as given by BTK,

$$T(E) = 1 + |a|^2 - |b|^2, \quad (15)$$

depends only on the combination

$$Z_{\text{eff}}^2 = Z^2 + \frac{(r-1)^2}{4r} = \frac{(r_{\text{eff}}-1)^2}{4r_{\text{eff}}}. \quad (16)$$

Thus, this result, given by Blonder and Tinkham⁷ for the $l=0$ case, is valid also for finite l . Hence, the two limiting cases,

$$v_F^> = v_F^<, \quad (17)$$

i.e., $r=1$, $Z \neq 0$ (δ -function scattering only), and

$$r \neq 1, \quad Z=0$$

(Fermi-velocity misfit only), are extended to the general case in the same way as in the $l=0$ case, namely by either replacing Z by Z_{eff} , or r by r_{eff} , as given in (16). Since we concentrated on the second case in the early stages of our analysis, and thus (rather fortuitously) our preliminary report (HL) and all numerical work was based on using the parameter r_{eff} instead of Z_{eff} , we retain this use of r_{eff} , the corresponding Z_{eff} simply being given by (16).

The final result for the transmission coefficient as a function of reduced energy,

$$\eta = E/\Delta, \quad (17)$$

is obtained from (4), (5), (10)–(13), (15), and (16), and can be expressed in the form

$$T(\eta) = \begin{cases} 2/(1+S\{1-\cos[2(\lambda\eta-\arccos\eta)]\}) & \text{for } \eta < 1, \\ T_\infty[1+(1-P)x-Px^2]/[1+P^2x^2-2Px\cos(2\lambda\eta)] & \text{for } \eta > 1, \end{cases} \quad (18)$$

using the following abbreviations:

$$x = [\eta - (\eta^2 - 1)^{1/2}]^2, \quad P = \left[\frac{r-1}{r+1} \right]^2, \quad (19)$$

$$S = \frac{(r^2-1)^2}{8r^2}, \quad T_\infty = T(\infty) = \frac{4r}{(r+1)^2}.$$

Apart from a numerical factor $2/\pi$,

$$\lambda = 2\Delta l / \hbar v_F = (2/\pi)(l/\xi) \quad (20)$$

is the "melting depth" in units of the coherence length ξ .

r must be read as r_{eff} , the index being dropped for simplicity here and in what follows. In addition, numerical Z values given later must be read as Z_{eff} . As may easily be realized, Eqs. (18)–(20) constitute the result given without derivation in another form by HL (this result being corrected, as indicated in Ref. 4).

The interference effects represented by the cosine terms in the denominators of (18) are, of course, not unexpected. Their analogs under somewhat differing boundary conditions and for somewhat differing physical problems have been theoretically investigated for $\eta < 1$ in the work by de Gennes and Saint-James as early as 1963,⁸ and for the case of general η they lead to the well-known Rowell-McMillan⁹ oscillations in the quasiparticle density of states of normal-metal–superconductor sandwich structures. While the emphasis was on the density of states in these investigations, the normal-metal–superconductor system being separated from its surroundings by either an infinite potential step or by a tunneling barrier of extremely low transmission, we here instead followed the BTK method of handling the open system of a metallic contact with small amount of normal scattering by calculating an energy-dependent overall current-transmission coefficient.

III. SAMPLES AND EXPERIMENTAL RESULTS

The experimental results only briefly described in HL and to be analyzed in Sec. IV were obtained as a by-product of several years of research on tunnel junctions prepared on bulk tantalum.¹⁰ During these investigations, a total of several hundreds of junctions were prepared by the same techniques to be described below, and with the same sort of counter contact, namely an evaporated silver film typically 1000 Å thick. More than 90% of the junctions showed typical tunneling behavior. A small percentage of samples, however, obviously contained metallic links. It is the properties of these samples we are dealing with in this paper.

Sample preparation was as follows: The tip of a 0.4-mm-diam tantalum wire is carefully out-gassed with the aid of electron-gun heating under ultrahigh-vacuum conditions and at a temperature slightly below the melting

point. Finally, the tip is melted into a hanging drop to produce a smooth surface, and then cooled to room temperature. The sphere-shaped molten drop crystallized in single-crystal form. Residual-resistivity ratios after this treatment are typically 10 000 or higher.

After breaking the vacuum, the sample is air-oxidized at room temperature for 10–60 min, and, after masking a 0.1×0.1 mm² tunneling window with Formvar paint, a silver counter electrode is evaporated. After contacting a gold wire to the silver film, the sample is mounted on a suitable sample holder and immersed in a helium-bath cryostat to measure the current-voltage characteristics and its derivative with the usual Adler-Jackson¹¹ modulation techniques.

Although only a small percentage of the samples contained metallic links, the final number of these was more than 20 on account of the large overall number of samples.

While a detailed account of the entire experimental material obtained by the author and several members of our experimental group lies beyond the scope of this article,¹² the general findings can easily be described on the basis of the example already presented by HL and quantitatively to be analyzed in Sec. IV. For illustration of the following statements, the reader may glance at the experimental curve represented in Fig. 4. The following observations were made at 1.6 K, the lowest measuring temperature:

(1) Normal-state resistance was typically 0.2–1 Ω, in contrast to 10 to several hundred Ohms for tunneling junctions.

(2) Normal-state conductance decreased slightly with bias, as is typical for metallic contacts,¹³ in contrast to tunneling behavior.¹⁴

(3) In the superconducting state, conductance was larger than in the normal state in the gap region $eU \lesssim \Delta$, with a relative minimum at zero bias observed in most cases, this minimum still corresponding to about 1.1–1.4 times the normal-state conductance. Thus the low-bias behavior is in rough agreement with the BTK theory for a small Z parameter of about 0.5, and, in fact, this observation, when first made, was a key to an understanding of our experimental results.¹⁵

(4) In a higher-bias regime, situated somewhere between 3 and 15 mV and typically extended over several millivolts, two stable states existed under our condition of constant imposed current. One of these states was continuously reached from the low-bias regime and the other from the high-bias regime, with the entire phenomenon representing a hysteretic transition between two clearly separated states, which shall be termed the "low-" and "high-injection-current" states. The low-injection-current state always represented a smooth variation of conductance with voltage, coming rather close to the behavior which other authors observed for low-resistance point contacts, with deviations from the BTK prediction ac-

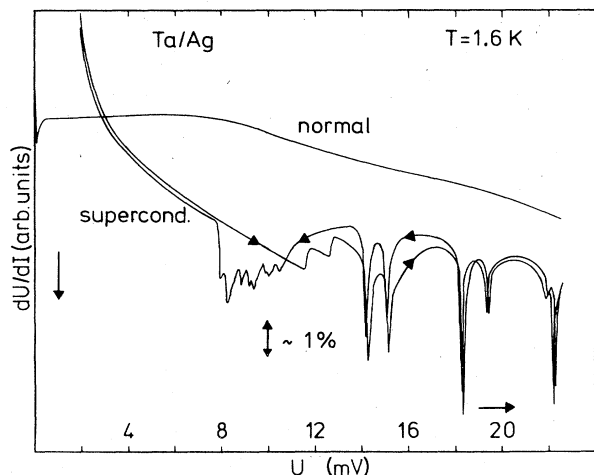


FIG. 2. Differential resistance of a Ta/Ag metallic contact. Normal-state resistance was $R_N=0.2 \Omega$, and the normalized excess current $eR_N\Delta^{-1}(I_S-I_N)\approx 0.55$ for $2 \text{ mV} < U < 8 \text{ mV}$.

counted for by heating.^{7,16}

While statements (1)–(4) hold for all of the samples, the high-bias state which we are mainly interested in represented itself rather differently for different samples. In any case, strong structures were observed in the first derivative, dI/dU ; the shape of these structures, however, was rather different. Only in a few cases were rather smooth oscillations of the kind represented in Fig. 4 observed. In other cases, a nearly periodic pattern was observed in dI/dU , but with rather sharp and narrow minima, far from what might be called a damped harmonic behavior. An example of this kind is represented in Fig. 2, taken from unpublished work by H. Lerchner and the author. While Figs. 2 and 4 represent extreme cases, there are examples intermediate between them. Upon close examination, the feature of a narrow minimum and broad neighboring maxima, say, the “anharmonicity” typical of Fig. 2, is also seen in Fig. 4 for the minimum at 8 mV.

We feel that examples such as that represented in Fig. 4 give a better chance of approaching an understanding of the physics of the high-injection-current state, and, hence, in the next section, we perform an analysis of this example along the lines already presented by HL, i.e., assuming a “melting depth” driven to higher and higher values by increasing injection.

IV. NUMERICAL RESULTS AND COMPARISON WITH EXPERIMENT

Any attempt to understand the observed structures as a result of some fixed-geometry–variable-energy resonance, say, of the Rowell-McMillan type, would quantitatively fail. The reason is, simply, that $eU \gg \Delta$ holds in the observation regime, and, thus, corresponding contributions, falling off with energy eU like $(\Delta/eU)^2$, prove to be smaller than the observed effects by an order of magnitude or even more. In contrast to this, alterations of the excess current by variations of the geometry of the supranormal transition are, in principle, observable at arbitrarily high

voltage, the reason being that the excess current at any high voltage is largely determined by the low-energy contributions to the current integral.

Thus we are interested in the excess current at very high voltage U —in fact, its $U \rightarrow \infty$ limit defined by BTK in normalized form as

$$\hat{I}_{\text{exc}} = \frac{eR_N}{\Delta} \lim_{U \rightarrow \infty} [I_S(U) - R_N^{-1}U], \quad (21)$$

which can be calculated from the current-transmission coefficient, for given normal scattering and normalized “melting depth” λ , as

$$\hat{I}_{\text{exc}} = \int_0^\infty \frac{T(\eta) - T_\infty}{T_\infty} d\eta. \quad (22)$$

We have numerically calculated \hat{I}_{exc} for several values of r and $0 \leq \lambda \leq 5\pi$, the result being represented in Fig. 3. As expected, oscillations are observed in all cases except in the $r=1$ and the $r \rightarrow \infty$ limits.

The experimental conductance, normalized to the normal conductance R_N^{-1} , should be given by

$$R_N \left[\frac{dI}{dU} \right]_{\text{expt}} = \frac{\Delta}{e} \frac{d\hat{I}_{\text{exc}}}{d\lambda} \frac{d\lambda}{dU}, \quad (23)$$

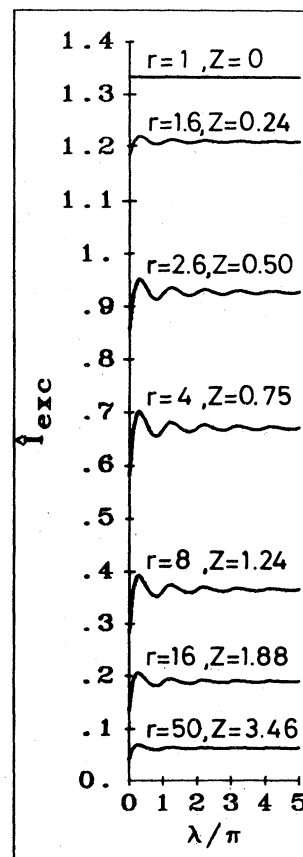


FIG. 3. Normalized excess current vs normalized “melting depth” calculated by numerical integration.

with $\lambda(U)$ representing the bias dependence of the melting depth $l = (\pi/2)\lambda\xi$.

In Fig. 4 we display the positive bias part of the experimental dU/dI characteristics already presented by HL. Here, we are only interested in the high-injection-current branch, which clearly represents four minima at different U values. By tentatively identifying these with the first four minima in $d\hat{I}_{\text{exc}}/d\lambda$ calculated as a function of λ , a scale is given relating λ and U , this relation being represented by the four dots in the inset of Fig. 4. Although this relation deviates from linearity, we may neglect this nonlinearity as a first approximation and assume the linear $\lambda(U)$ dependence indicated by the straight line in the inset of Fig. 4. After doing so, we can calculate the right-hand side of Eq. (23) for given r without any further parameter fit, the factor $d\lambda/dU$ being given by the slope of that straight line. With $r=2.6$, corresponding to $Z=0.5$, taken from the low-injection-current behavior according to HL, we obtain the theoretical curve in Fig. 4 representing the right-hand side of Eq. (23). Δ was taken to be 0.72 meV.¹⁰ The display is such that not only the λ - and U -abscissa scales of the experimental and theoretical curves are linearly related, as described above, but also the ordinate scale is chosen so as to correctly represent the relative variations of the experimental conductance in the high-injection-current regime (a few percent at most). Thus the amplitudes of experimental and calculated oscillations can be directly compared.

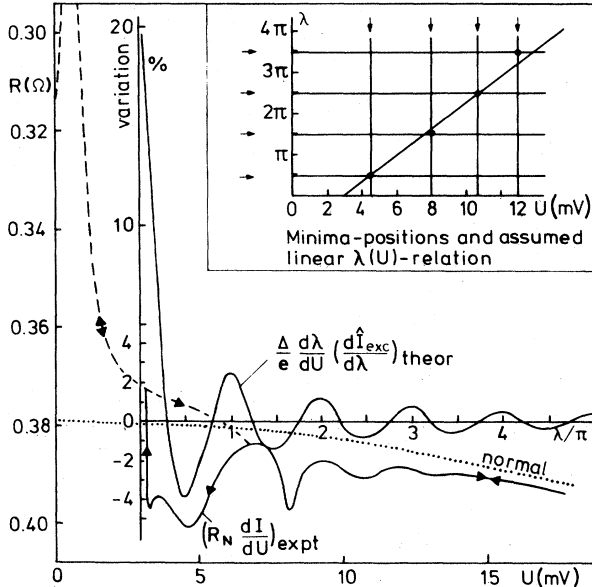


FIG. 4. Dashed and lower solid curves: Differential resistance R vs voltage U of a Ta/Ag metallic contact in the low- and high-injection-current regimes, respectively. Below 3.16 mV only the low-injection-current state is stable; above 6.8 mV only the high-injection-current state is stable. Dotted curve: R vs U in the normal state. Second ordinate scale: with respect to this scale, the lower solid curve represents $R_N(dI/dU)$, i.e., experimental conductance normalized to zero-bias normal-state conductance. Upper solid curve: Theoretical normalized conductance, for $r=2.6$, vs melting depth, or vs U (see inset and text).

As a result, the amplitudes of the oscillations corresponding to the lowest-order interferences are represented appreciably better than might have been expected from the simple model from which, at most, an order-of-magnitude agreement was expected before the calculations were done. It should be emphasized that the theoretical-curve amplitude does not contain any adjusted parameter, the r value being adopted from the low-injection-current state in a manner to be described more precisely below. The higher-order interferences are somewhat less pronounced experimentally than theoretically predicted, and no further structure was resolved experimentally beyond the fourth minimum.

We claim that the good representation of the low-order-interference amplitudes by the theory strongly indicates that the physics of the model is basically correct. One might ask, therefore, how safe the chosen r value is, and how strongly alterations of r , within reasonable limits, would modify the theoretical result.

HL obtained $Z=0.5$, i.e., $r=2.6$, on the basis of the BTK theory from the measured value of the superconducting-to-normal zero-bias resistance ratio at 1.6 K. As mentioned in that paper, some deviations from the BTK prediction occurred at higher bias, typical for low-resistance junctions and attributed to heating effects.^{7,16} In fact, higher r values are obtained from the normalized excess current

$$\hat{I}_{\text{exc}}(U) = eR_N\Delta^{-1}[I_S(U) - I_N(U)]$$

directly measured at $U \gg \Delta/e$. In the (3–8)-mV regime typical for the lowest-order interferences in Fig. 4, one ob-

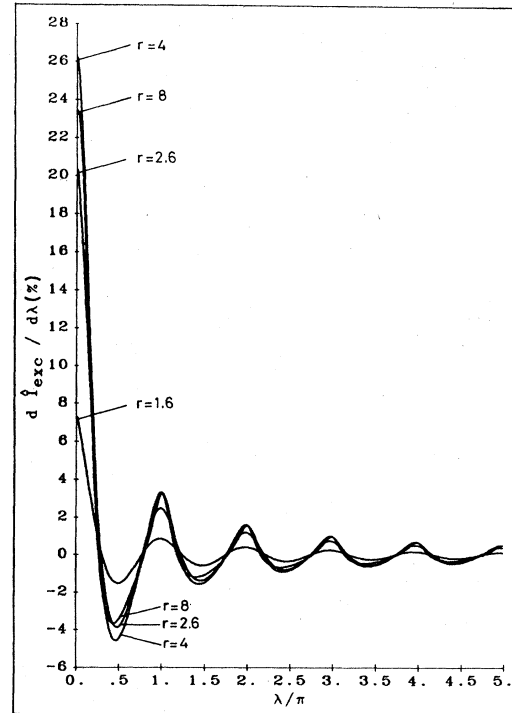


FIG. 5. $d\hat{I}_{\text{exc}}/d\lambda$ vs λ for different values of normal scattering parameter r . Dependence on r is only weak for $2.6 \leq r \leq 8$.

tains $\hat{I}_{\text{exc}}(U) \approx 0.4$ from the data represented in Fig. 1 of HL. This corresponds to values somewhat below $r=8$ or $Z=1.24$, and, hence, appreciably larger than the values obtained from the zero-bias resistance ratio.

As a matter of fact, however, the theoretical $d\hat{I}_{\text{exc}}/d\lambda$ curve only very slightly depends on r for r values between 2.6 and 8. This peculiarity is seen in Fig. 5, representing $d\hat{I}_{\text{exc}}/d\lambda$ vs λ for some r values as calculated numerically with high precision. Hence the good agreement between experiment and theory claimed above is not at all affected by some uncertainty regarding the most adequate value of the r parameter, since any reasonable r value yields practically the same result as the value chosen in Fig. 4.

V. DISCUSSION

We postpone discussion of the most important point, namely the three dimensionality of the experimental situation in contrast to the one-dimensional model, to the end of this section.

There are two deviations of minor importance between experimental and theoretical results as represented by the solid curves of Fig. 4. Firstly, the small size of the experimental fourth-order—interference minimum and the nonobservability of higher orders can be accounted for by several reasons, the most probable being small deviations from the geometry, which allows for constructive or destructive interference. Another possible explanation would be in terms of a finite quasiparticle mean free path of several coherence lengths order of magnitude.

Secondly, the downward shift of the experimental with respect to the theoretical curve is of little importance. It could have been somewhat reduced by normalizing the experimental conductance with respect to the voltage-dependent, instead of the zero-bias, normal conductance. The remaining discrepancy is due to the fact that, apart from the oscillations, the mean excess current slowly decreases with increasing bias. This effect, clearly observable from the experimental current-voltage characteristics (see HL), cannot be accounted for by the simple model, but most also be expected for a finite quasiparticle mean free path.

A third discrepancy concerns what was, in Sec. III, already called the “anharmonicity” of the experimental curve. Clearly, this can easily be accounted for by assuming a nonlinear instead of a linear $\lambda(U)$. What must be concluded from the experimental result of Fig. 4 within the framework of the given interpretation, is that near $\lambda=3\pi/2$ (the position of the second dI/dU minimum) the “melting depth” varies more quickly with voltage U than it does in the neighboring regions around $\lambda=\pi$ and $\lambda=2\pi$.

We are seriously confronted here with the fact that the description given is essentially phenomenological, and that no self-consistent theory is available to explain the spatial variations of pair potential and electric field under the condition of externally controlled current injection.

While any attempt to improve this situation lies beyond the scope of this investigation, some conclusions and suggestions concerning the high-injection-current state can be drawn from the experimental observation.

Firstly, there are apparently rather strong nonlinearities in the dependence of melting depth on bias, Fig. 2 representing an extreme example. It is highly probable that the same sort of nonlinearities constitute the source of bistability in the hysteretic transition regime between the low- and high-injection-current states that was observed for all samples.

A second conclusion is based on the observation that in the high-injection-current state, and even in the hysteretic transition regime, the total variation of conductance is only a few percent of the normal-state conductance, despite the strong nonlinearities. From this observation, one may conclude that Joule heating by the total (normal plus excess) current is not the main mechanism driving the “melting depth.” This is in contrast with the view underlying our previous paper (HL), in which this argument had been overlooked.

Finally, one might ask why a one-dimensional model should be applicable to a truly three-dimensional problem. In fact, the diameter of the orifice connecting both metals is rather small compared with the “melting depth,” say, at the fourth minimum of the curves in Fig. 4. An easy estimate leading to this conclusion is as follows:

Firstly, from the pure-tantalum low-temperature coherence length $\xi=925 \text{ \AA}$,^{17,18} one obtains $l_1=(\pi/2)\lambda_1\xi=(\pi/2)^2\xi=2300 \text{ \AA}$ for the l value at the first minimum, and 7 times this value at the fourth minimum.

On the other hand, the orifice diameter d may be obtained from the normal-state resistance R_N with the aid of the formula given by BTK and essentially representing a generalization of the Sharvin formula¹⁹ to include elastic scattering as described by the parameter Z , namely

$$R_N^{-1}=2N(0)e^2v_F\frac{\pi}{16}d^2(1+Z^2)^{-1}. \quad (24)$$

From typical values of the Fermi velocity v_F and one-spin density of states $N(0)$, in metals, one typically obtains $d=800 \text{ \AA}$.

Hence, at least for the higher-order interferences, d is small compared to l . One must then think of the normal phase as forming some kind of droplet in the tantalum half-space centered around an injection orifice of small spatial extent. It is very important that, regardless of the exact shape of this droplet, Andreev reflection focuses back on the injection orifice on account of the special nature of Andreev reflection, which conserves momentum and, hence, transforming an electronlike to a holelike excitation and vice versa, simply inverts the group velocity of quasiparticles on account of time-reversal symmetry. Hence, the trajectories of incoming electrons and reflected hole wave packets are identical even if the reflecting phase boundary is not orthogonal to this trajectory. Thus a one-dimensional model does not seem as bad an approximation as it might first appear for a calculation of the amplitude of the interference oscillations. In order to obtain fully constructive or destructive interference, one must then, of course, assume that the phase boundary approximately is at a constant distance from the injection hole, i.e., that the droplet shape does not deviate too much from a half-sphere. This assumption seems quite reasonable for an injection orifice of small spatial extent, say, a

pointlike injection hole, if one additionally assumes random normal scattering in the orifice, i.e., the random nature of the scattering described by the scattering parameter Z of the model.²⁰ In this case, the entire problem is approximately spherically symmetrical, since cooling through the sample surface is negligible compared with heat conduction to the bulk.²¹ It is important, however, that even small deviations from spherical droplet shape (although they might lead to some reduction in interference amplitude) do not affect focusing conditions in the case of Andreev reflection, as they seriously would for normal reflection, which does not invert, but rather conserves, the tangential components of group velocity.

In fact, for a one-dimensional instead of random current injection, another more serious difficulty would arise in justifying the simple model, namely the following:

According to BTK, the $E < \Delta$ contributions to the current integral are converted from quasiparticle current to supercurrent within a damping length given by the reciprocal of the imaginary part of κ^\pm as given in (4). This is easily found to take a minimum value $\pi\xi$ at $E=0$, and although it increases to infinity when E approaches Δ , a scale of a few coherence lengths is thus given for this current conversion. Within this scale, the current density corresponding to the $E < \Delta$ contributions must have fallen off to values that are small compared with the critical current as calculated for a homogeneous current-carrying state,^{5,6} otherwise (in our treatment) use of a real pair potential $\Delta(x)$ would have been disallowed. As an easy estimate shows, unless $Z \gg 1$, the current density does not meet this smallness requirement at the orifice and, consequently, would not meet it anywhere in a one-dimensional geometry. Instead, three-dimensional spreading is essential to justify the assumption of the pair condensate essentially at rest.

In contrast with the analyzed experimental example where the assumption of negligible supercurrent density seems to work, it may be inapplicable in other cases. Progress might be possible in understanding more aspects of

the involved experimental results by an attempt to avoid this assumption, i.e., looking for a complex self-consistent solution for the pair potential under injection conditions. It is hoped that such an effort might finally lead to an understanding of the systematics, which are doubtless present in experimental results such as that represented in Fig. 2, but which are not presently understood. The simple phenomenological approach given here to discuss the simpler empirical case of Fig. 4 might thereby serve as a hint that Andreev reflection by the spatially inhomogeneous "supranormal" structure (or, more generally speaking, interference of low-energy quasiparticles within the geometry of this structure) might be important for the self-consistent nonlinear theory to be developed. The final result might thereby well present richer structure of nonequilibrium states than the simple normal droplet here assumed. As an example, one could imagine finding time-dependent structures or stationary, spatially inhomogeneous phases similar to those found in flat film geometries.²² In contrast to the film geometry, the results reported by HL and this paper are characterized by quite different geometrical and cooling conditions, and they thus correspond to a very different situation with respect to phonon escape times and quasiparticle elastic mean free path. As far as the author is aware, they constitute the first results on nonequilibrium in a high-purity half-space with approximately pointlike quasiparticle injection.

ACKNOWLEDGMENTS

This work has benefited much from discussion of unpublished experimental results by H. Lerchner, H. Ekruť, M. Brunner, and R. Kůke. R. Kůke and S. Hahn performed most of the extensive numerical calculations. A clarifying discussion on a particular metallurgical problem with Prof. Dr. E. Kneller is greatly appreciated. Part of the experimental work was supported by the Deutsche Forschungsgemeinschaft.

¹A. Hahn and H. Lerchner, in *Proceedings of the 17th International Conference on Low Temperature Physics, Karlsruhe, 15–22 August, 1984*, edited by U. Eckern, A. Schmid, W. Weber, and H. Wůhl (North-Holland, Amsterdam, 1984), Pt. II, DL 9, p. 803. This paper is referred to as HL in the text.

²G. E. Blonder, M. Tinkham, and T. M. Klapwijk, *Phys. Rev. B* **25**, 4515 (1982), referred to as BTK in the text.

³A. F. Andreev, *Zh. Eksp. Teor. Fiz.* **46**, 1823 (1964) [*Sov. Phys.—JETP* **19**, 1228 (1964)]. Also see Refs. 8 and 9.

⁴Reference 1 (HL) contains a wrong sign in the last equation of system [1a] where γ_1 has to be replaced by $-\gamma_1$. Equation [4] of HL must be replaced by the correct definition of δk as given in (4) of the present paper.

⁵P. G. de Gennes, *Superconductivity of Metals and Alloys* (Benjamin, New York, 1966), Chap. 5.

⁶M. Tinkham, *Introduction to Superconductivity* (McGraw-Hill, New York, 1975), Chap. 8-1. For choosing a real Δ , see last two paragraphs of Sec. V.

⁷G. E. Blonder and M. Tinkham, *Phys. Rev. B* **27**, 112 (1983); G. E. Blonder, Ph.D. thesis, Harvard University, 1982.

⁸P. G. de Gennes and D. Saint-James, *Phys. Lett.* **4**, 151 (1963).

⁹J. M. Rowell and W. L. McMillan, *Phys. Rev. Lett.* **16**, 453 (1966).

¹⁰K. Gůrtner and A. Hahn, *Z. Naturforsch.* **31a**, 858 (1976); H. Ekruť and A. Hahn, *J. Appl. Phys.* **51**, 1686 (1980); M. Brunner, H. Ekruť, and A. Hahn, *ibid.* **53**, 1596 (1982); A. Hahn, H. Ekruť, and M. Westphal, *Phys. Rev. B* **26**, 138 (1982); A. Hahn, M. Brunner, and H. Ekruť, *Thin Solid Films* **102**, 221 (1983); M. Brunner, H. Ekruť, and A. Hahn, *Solid State Commun.* **46**, 259 (1983).

¹¹J. G. Adler and J. Jackson, *Rev. Sci. Instrum.* **37**, 1046 (1966).

¹²Unpublished work by the author and H. Lerchner, H. Ekruť, M. Brunner, and R. Kůke.

¹³A. G. M. Jansen, A. P. van Gelder, and P. Wyder, *J. Phys. C* **13**, 6073 (1980).

¹⁴Although in all our experiments the recorded signal is the differential resistance, we prefer to discuss its reciprocal, since the conductance is closely related to physical quantities, e.g., density of states for tunneling junctions and transmission coefficient for metallic contacts. In representing experimental

results (Figs. 2 and 4), the directly registered resistance is plotted downward along the ordinate axis. Since variations are small in most cases, the corresponding curves can, with negligible error, be interpreted as representing the conductance along the positive ordinate axis. By this, the parallel use of both ordinate scales in Fig. 4 for the same curve is also justified.

- ¹⁵In some cases, the behavior in the gap region was more complicated. In all cases, however, conductance was larger than in the normal state leading to a finite excess current at higher bias.
- ¹⁶G. Voss, Ph.D. thesis, Universität Köln, 1984.
- ¹⁷I. P. McEvoy, D. P. Jones, and J. G. Parks, *Phys. Rev. Lett.* **22**, 229 (1969).
- ¹⁸J. Auer and H. Ullmaier, *Phys. Rev. B* **7**, 136 (1972).
- ¹⁹Yu. V. Sharvin, *Zh. Eksp. Teor. Fiz.* **48**, 984 (1965) [*Sov. Phys.—JETP* **21**,655 (1965)].
- ²⁰If the spatial extent of the scattering region is small compared with ξ , this randomness does not destroy coherence.
- ²¹M. Tinkham, in *Nonequilibrium Superconductivity, Phonons, and Kapitza Boundaries*, edited by K. E. Gray (Plenum, New York, 1981), p. 231.
- ²²I. Iguchi, in *Proceedings of the 17th International Conference on Low Temperature Physics, Karlsruhe, 15–22 August, 1984*, edited by U. Eckern, A. Schmid, W. Weber, and H. Wühl (North-Holland, Amsterdam, 1984), Pt. III, and references given therein.